Nuclear pasta in hot dense matter and its implications for neutrino scattering

Alessandro Roggero, Jérôme Margueron, Luke F. Roberts, and Sanjay Reddy

Phys. Rev. C **97**, 045804 — Published 16 April 2018

DOI: 10.1103/PhysRevC.97.045804

INT-PUB-17-045, LA-UR-17-29841

Nuclear pasta in hot dense matter and its implications for neutrino scattering

Alessandro Roggero*
Institute for Nuclear Theory, University of Washington, Seattle, WA 98195
Theoretical Division, Los Alamos National Laboratory, Los Alamos, New Mexico 87545, USA

Jérôme Margueron†
Institute for Nuclear Theory, University of Washington, Seattle, WA 98195
Institut de Physique Nucléaire de Lyon, CNRS/IN2P3, Université de Lyon, Université Claude Bernard Lyon 1, F-69622 Villeurbanne Cedex, France

Luke F Roberts‡
National Superconducting Laboratory & Department of Physics and Astronomy, Michigan State University, East Lansing, MI 48824, USA

Sanjay Reddy§
Institute for Nuclear Theory, University of Washington, Seattle, WA 98195
(Dated: March 23, 2018)

The abundance of large clusters of nucleons in neutron-rich matter at sub-nuclear density is found to be greatly reduced by finite temperature effects when matter is close to beta-equilibrium, compared to the case where electron fraction is fixed at $Y_e > 0.1$ as often considered in the literature. Large nuclei and exotic non-spherical nuclear configurations called pasta, favored in the vicinity of the transition to uniform matter at $T = 0$, dissolve at relatively low temperature $T_{\rm u}$ as protons leak out of nuclei and pasta. For matter in β-equilibrium with a negligible neutrino chemical potential we find that $T_{\rm u}^{\beta} \simeq 4 \pm 1$ MeV for realistic equations of state. This is lower than the maximum temperature $T_{\rm max}^{\beta} \simeq 9 \pm 1$ MeV at which nuclei can coexist with a gas of nucleons, and can be explained by a change in the nature of the transition to uniform matter called retrograde condensation. An important new finding is that coherent neutrino scattering from nuclei and pasta makes a modest contribution to the opacity under the conditions encountered in supernovae and neutron star mergers. This is because large nuclear clusters dissolve at most relevant temperatures, and at lower temperatures when clusters are present, Coulomb correlations between them suppresses coherent neutrino scattering off individual clusters. Implications for neutrino signals from galactic supernovae are briefly discussed.

I. INTRODUCTION

The properties of hot dense matter encountered in core-collapse supernovae, newly born neutron stars called proto-neutron stars, and in neutron star mergers is expected to play a key role in shaping their observable photon, neutrino and gravitational wave emission. In supernovae, state of the art simulations indicate that neutrino transport at high density influences the supernova mechanism [1, 2], the long term neutrino emission detectable in terrestrial neutrino detectors [3–6], and heavy element nucleosynthesis [7–11].

The presence of heterogeneous matter at high density is expected to modify the neutrino scattering rates because the size of structures encountered in such matter can be comparable to the neutrino wavelength, and neutrinos would couple coherently to the net weak charge contained within them. A familiar example is neutrino-nucleus coherent scattering, known to play an important role in trapping neutrinos during core-collapse [12]. Additionally, heterogeneous phases are favored near first-order phase transitions in neutron stars at high density [13], and coherent neutrino scattering in such matter can greatly increase the opacity [14]. Coherent neutrino scattering from the nuclear pasta phase where large spherical and non-spherical nuclei coexist with a dense nucleon gas for densities between $10^{13} - 10^{14}$ g/cm^3 has also been studied [15, 16].

Recently, the enhanced neutrino opacity in the high density heterogeneous pasta phase was incorporated in simulations of proto-neutron star evolution and found to have a significant impact on the temporal structure of the neutrino luminosity [17]. Motivated by this interesting finding, we perform calculations of matter at finite temperature to address if heterogeneous nuclear pasta is present under the typical thermodynamic conditions encountered in proto-neutron stars, and study its influence on the neutrino scattering rates. We find that the heterogeneous pasta phase dissolves at relatively low temperature for the small values of the electron fraction characteristic of dense matter in beta-equilibrium. Consequently, the enhancement of neutrino scattering rates due to coherent scattering is relatively modest and significantly smaller than those employed in [17]. In ad-

* roggero@lanl.gov
† jmargue@uw.edu
‡ robertsl@nscl.msu.edu
§ sareddy@uw.edu

dition, we find that Coulomb correlations between clusters suppresses scattering of neutrinos with wavelengths larger than the inter-cluster distance in agreement with earlier work [18, 19]. Interestingly, we also find that at lower temperatures when large nuclei can be present there could be a net reduction of the neutrino opacity as nucleons get locked up inside nuclei.

The material is organized as follows. In §II we review the basic nuclear physics of phase coexistence and show that the simplified Gibbs construction for two-phase equilibrium provides a useful bounds on the phase boundaries between homogeneous and heterogeneous matter. This allows us to provide an upper limit on the critical temperature above which pasta dissolves to form a uniform nucleon liquid, and its dependence on the nuclear equation of state is discussed. Implications for neutrino transport in proto-neutron stars are discussed in §III, and our conclusions are presented in §IV.

II. HOT MATTER AT SUB-NUCLEAR DENSITY AND THE DISSOLUTION OF PASTA

The structure of matter at sub-nuclear density and zero temperature is fairly well understood [45]. With increasing density, nuclei become neutron-rich due to the rapid increase in the electron Fermi energy. Neutrons drip out of nuclei when the density exceeds $\rho_{\rm drip} \simeq 4\times10^{11}$ g/cm^3, and non-spherical or pasta nuclei are likely when the density exceeds $\rho_{\rm pasta} \simeq 10^{13}$ g/cm^3 [20]. Several studies using different many-body methods and underlying nuclear interactions have all yielded similar qualitative behavior [20–22].

At finite temperature, the situation is less clear. Some calculations indicate that at the highest densities, nuclei and pasta persist up to $T \simeq 10-15$ MeV when the electron (or proton) fraction $\rm Y_e \gtrsim 0.1$ [23, 24]. Others find that the large and coherent structures, such as rod, tubes, and planes disappear at much lower temperature [47, 49].

In what follows we shall derive an upper bound on the temperature for the dissolution of nuclei and pasta for beta-equilibrated matter at densities in the range $\rho \simeq 10^{12} - 10^{14}$ g/cm^3. We show that the dissolution of clusters is related to a change in the nature of transition to the high density uniform phase, which turns from an ordinary gas-to-liquid transition, during which the volume fraction of the high density phase continues to increase, into a less ordinary gas-to-liquid-to-gas transition also called retrograde condensation where the volume fraction of the high density phase decreases [26]. To begin we consider beta-equilibrium matter with zero neutrino chemical potential because the outer regions of a proto-neutron star, which may contain nuclear pasta, are able to deleptonize rapidly and reach beta-equilibrium on a short time scale compared to the timescales of relevance to proto-neutron star evolution [3–6].

First, we identify the thermodynamic conditions favorable for the existence of nuclear pasta. Since surface and Coulomb energies act to disfavor the heterogeneous state, and shell effects are relatively small at the temperatures of interest, the liquid-gas phase coexistence region predicted by the Gibbs construction, where these effects are ignored, will likely enclose the phase coexistence region predicted when such finite size effects are included. This simple observation allows us to provide a useful upper bound on the dissolution temperature by examining the two-phase Gibbs construction for bulk matter. We note that neglecting finite size effects has been shown to provide results comparable to the Thomas-Fermi approach at finite temperature [48] (see Erratum of this reference), as well as those obtained from a quantum molecular dynamics calculation [49].

In the following, we briefly recall the well-known Gibbs construction applied to a nuclear system composed of neutrons and protons [24–26]. For nuclei or pasta to coexist with a gas of nucleons, the high density liquid phase inside these structures have to be in equilibrium with the low density gas outside. Denoting the pressure, and the neutron and proton chemical potentials of the high density liquid phase as P^h, and μ_n^h and μ_p^h, respectively, Gibbs equilibrium requires $P^h = P^l$, $\mu_n^h = \mu_n^l$ and $\mu_p^h = \mu_p^l$, where P^l, μ_n^l and μ_p^l, are the corresponding pressure and chemical potentials in the low density gas phase. To find the coexistence region in the phase diagram an equation of state which specifies how the energy density of bulk nucleonic matter $\varepsilon_{\rm nuc}(n_n, n_p, T)$ depends on the neutron and proton densities, and the temperature is needed. In practice we work in the proton-canonical ensemble where μ_n is fixed and n_p is the extensive variable [25]. We have however checked that our results are independent of the statistical ensemble.

At a fixed temperature, phase coexistence is possible when there exists two pairs of nucleon densities, denoted by n_n^h, n_p^h and n_n^l, n_p^l, that can satisfy the Gibbs equilibrium criteria. These pairs can be depicted as two points on a two-dimensional plot where the axes are neutron and proton densities. In Fig. 1 these points are calculated for the model SLy4 and appear on the solid-black curve. For a pair of points in Gibbs equilibrium, a Gibbs construction can be used to find the state of matter at intermediate densities. Therefore, a pair of points that satisfy Gibbs equilibrium define a curve through neutron-proton density space given by [46]

$$\begin{aligned} n_n &= u n_n^h + (1-u) n_n^l \\ n_p &= u n_p^h + (1-u) n_p^l, \end{aligned} \tag{1}$$

where u is fraction of the volume that is occupied by the high-density liquid phase. The thin purple curves represent these curves for pairs of select Gibbs equilibrium points. For example, in the middle panel of Fig. 1, the pair of end points defined by the intersection labeled l and h specify the neutron and proton densities of the low and high density phases, n_n^l, n_p^l and n_n^h, n_p^h, respectively. Clearly, Y_e varies along any Gibbs construction curve, so a constant Y_e curve crosses the Gibbs constructions of many Gibbs equilibrium pairs in the mixed-phase

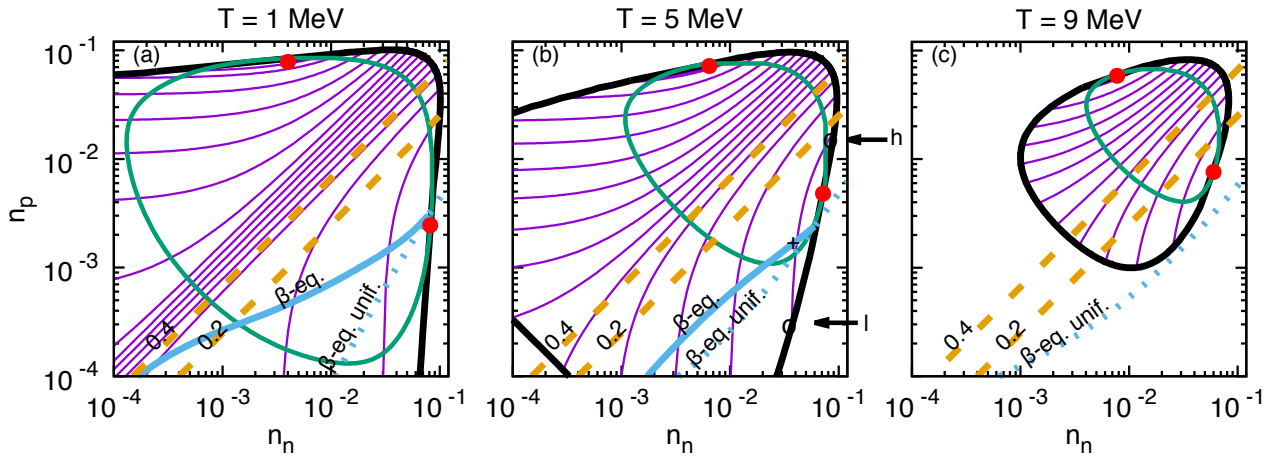

FIG. 1. β-equilibrium path (thick full blue line) for SLy4 Skyrme interaction in the coexistence region (delimited by the thick full black line) in the (n_n, n_p) plane and for T=1–9 MeV. A sample of the Gibbs construction paths are shown (thin full purple lines). The global density which intersect the β-equilibrium path line with the Gibbs construction one (see for instance the "+"symbol at T=5 MeV), represents the equilibrium state connecting the 2 phases at equilibrium which are located at the boundaries (see the points labeled l and h which are the low and high density phases associated to the global density identified by the "+" symbol at β-equilibrium). The constant Y_e = 0.2, 0.3 and 0.4 paths are represented by the thick yellow dashed lines. The spinodal instability region is also shown (thin full green line) and the critical points are shown with red solid dots with error-bars.

region. In Fig. 1, the yellow dashed lines show curves of constant Y_e and the Gibbs equilibrium at a specific Y_e is defined by its intersection with the purple curve. The thick-blue curve denotes the β-equilibrium path, along which $\mu_n - \mu_p = \mu_e$. Gibbs equilibrium is possible along the β-equilibrium path when thick-blue curve lies within the coexistence region. Once again, it can be seen that the β-equilibrium curve moves across many Gibbs equilibrium pairs as it traverses the coexistence region. The β-equilibrium path for the homogeneous phase is also shown as the dashed-blue curve for reference. The spinodal region where matter is unstable to small density perturbations is the region enclosed by the thin green curve, and the critical points associated with the first-order transition are denoted by the red dots.

Several insights about the role of finite temperature can be gleaned from examining the progression of the phase coexistence region with temperature seen in the three panels in Fig. 1:

- With increasing temperature the extent of the phase co-existence region shrinks, and its intersection with the path of β-equilibrium decreases. Above the critical temperature, $T^{\beta}_{\rm max}$ ($\simeq$ 9MeV for the model chosen) there is no intersection and phase coexistence in β-equilibrium is not possible.

- In contrast, out of β-equilibrium for moderate values of $Y_e > 0.2$ there exists a range of ambient conditions that extends to higher temperature where Gibbs equilibrium is possible. Nonetheless, with increasing temperature the area enclosed by the solid-black coexistence curve shrinks and its intersection with lines of constant Y_e is reduced. Eventually, above the critical temperature denoted by $T^{Y_e}_{\rm max} \simeq 12 - 15$ MeV there is no intersection and phase coexistence is absent.

- Co-existence in β-equilibrium ends near the critical point. With increasing temperature, phase co-existence ends by making a transition to the uniform low-density gas phase. This feature, called retrograde condensation [26], implies that the path along beta-equilibrium will favor fewer nuclei with increasing density.

- For moderate values of $Y_e > 0.2$ phase co-existence ends by transiting to the high-density liquid phase and large nuclei persist to higher temperature.

- With increasing temperature, the density contrast between the high and low density phases associated with Gibbs equilibrium is reduced.

The impact of retrograde condensation on the volume fraction of the high-density liquid phase is seen more clearly in Fig. 2. At low temperatures, u begins close

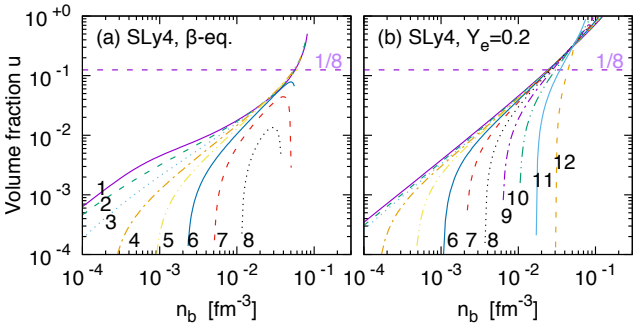

FIG. 2. Volume fraction of the high density phase in heterogeneous matter for SLy4 Skyrme interaction. (a) for the β-equilibrium path, (b) for the constant $Y_e = 0.2$ path.

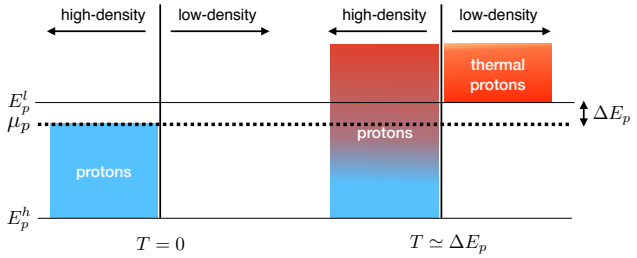

FIG. 3. This schematic shows the occupied proton energy levels in the low and high density phases that coexist in the heterogeneous phase. The $T = 0$ situation is shown on the left and finite temperature where a significant thermal population exists in the low density phase is on shown the right. See text for additional details.

to zero at low densities and increases to one at high densities, implying that it exits the coexistence region in the high-density phase. But above a critical temperature, u reaches a maximum of less than one and turns over, implying the β-equilibrium path exits the coexistence region in the low-density gas phase. The fact that the maximum volume fraction occupied by the high-density phase, which corresponds to nuclei or pasta structures, is rather small at temperatures high enough for retrograde condensation can significantly impact the contribution of coherent scattering to the neutrino opacity of β-equilibrium matter. Since non-spherical shapes or pasta nuclei are favored for $u \gtrsim 1/8$ (for a pedagogic discussion of pasta nuclei see Ref. [20]) we include the horizontal dashed line at $u = 1/8$ to help extract the critical temperature $T_{\rm u}^{\beta}$ above which pasta nuclei no longer appear (note that $T_{\rm u}^{\beta} < T_{\rm max}^{\beta}$). From panel (a) of Fig. 2 we see that $T_{\rm u}^{\beta}$ is between 5 and 6 MeV (for SLy4 EOS). In contrast for matter at fixed $Y_e = 0.2$, shown in panel (b), pasta nuclei persist to higher temperatures until phase coexistence ends at $T_{\rm max}^{Y_e}$

We can understand the physical mechanism for retrograde condensation at larger temperatures by examining the evolution of the proton fraction in the gas phase. Global charge neutrality ($n_e = n_p$) and Eq. (1) require the volume fraction of the high density phase to be

$$u = \frac{n_e - n_p^l}{n_p^h - n_p^l}\,, \tag{2}$$

where the electron density n_e is assumed to be uniform because the Debye screening length is large compared to the typical size of electrically neutral Wigner-Seitz cells. In the beta-equilibrium mixed phase the lowest energy level for protons in the low density gas phase $E_p^l > \mu_p$ and at $T = 0$ the proton density there denoted by $n_p^l = 0$. At $T = 0$ the volume fraction $u = n_e/n_p^h$ increases rapidly with increasing density because n_e increases and n_p^h decreases. At finite temperature $n_p^l > 0$ because proton states in the gas can be thermally populated. This is illustrated in Fig. 3 where the occupied energy levels of protons in both the low and high density phases are

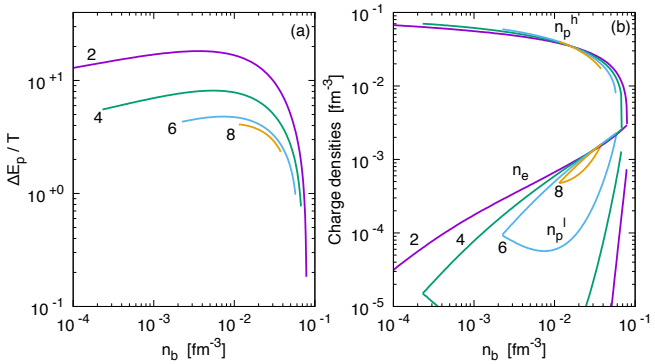

FIG. 4. (a) Energy differences $\Delta E_p/T$ and (b) charge particle densities (n_e, n_p^l, n_p^h) as function of the density and for different temperatures T = 1-6 MeV. The SLy4 EOS is considered here.

shown at zero and finite temperature.

The thermal population of protons in the gas [46]

$$n_p^l \simeq 2\left(\frac{m_p T}{2\pi}\right)^{3/2} e^{-\Delta E_p/T} \tag{3}$$

where $\Delta E_p = E_P^l - \mu_p$, becomes significant when $T \simeq \Delta E_p$ and increases exponentially with temperature. In contrast, the density of protons in the high density phase still remains significantly larger and does not change appreciably with temperature because of their high degeneracy.

The typical evolution of $\Delta E_p/T$ is shown in panel (a) of Fig. 4 for the SLy4 EOS. Except close to the transition density, $\Delta E_p/T \gg 1$ leads to significant suppression of the proton density in the gas phase. In the vicinity of the transition density $\Delta E_p/T$ decreases rapidly and from Eq. (3) the proton fraction in the gas increases exponentially. The number densities of the charged particles as function of the average baryon density are shown in panel (b). Since electric charge neutrality in the uniform phase requires $n_e = n_p = n_p^{gas}$, the point at which n_e and n_p^l first intersect defines the low density boundary of the

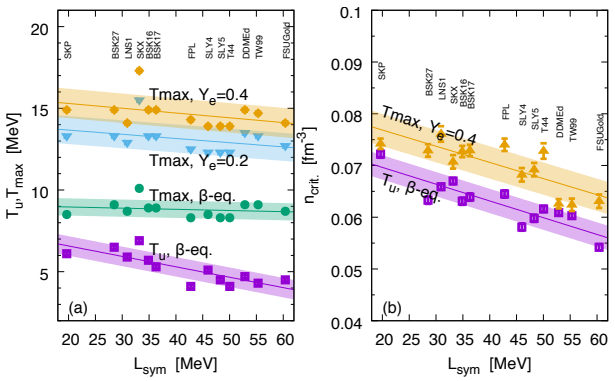

FIG. 5. (a) dissolution temperature $T_{\rm u}$ and maximal temperatures T_{max} at β-equilibrium, compared to T_{max} at fixed x_e=0.2 and 0.4 for the set of EOS compatible with chiral EFT EOS in neutron matter. (b) Highest density reached by the pasta phase for beta equilibrium or at fixed Y_e. These predictions are shown versus L_{sym}.

coexistence region. In the vicinity of this point, nonuniform matter is predominantly composed of the gas phase. The high density boundary is defined by the intersection of the n_e and n_p^h at low temperature, or by the second intersection of the n_e and n_p^l at high temperature as expected for retrograde condensation. These features are also readily discernible from Fig. 2 where the evolution of the volume fraction of the high density phase with density is shown for various temperatures.

As expected from the preceding discussion and Eq. (2), for matter in β-equilibrium where Y_e is small, the volume fraction u will decrease with density for $T \gtrsim \Delta E_p$. When this criterion is met, the density of protons in the low density gas phase will become comparable to the electron density, and eventually as ΔE_p decreases with density the volume fraction $u \to 0$.

We now turn to study the model dependence of the critical temperatures denoted by T_m^β, $T_{\rm max}^\beta$, and $T_{\rm max}^{Y_e}$ discussed earlier. We first select a subset of model Skyrme and relativistic mean field EOSs which predict the energy per particle of neutron matter at $n_b = 0.06$ and 0.10 fm^{-3}) that are compatible with QMC [27] or MBPT [28], which are based on two and three body chiral EFT potentials. The pasta dissolution temperature T_u^β for these models are shown in panel (a) of Fig. 5. The names of the EOS are shown vertically above the predictions and the EOS are ordered according to the slope of the symmetry energy at nuclear saturation density denoted by L_{sym}. The average prediction is $T_u^\beta = 5.0 \pm 2$ MeV and decreases with L_{sym} (the anti-correlation coefficient is -0.81) and the dispersion reflects the additional dependence on the EOS parameters. In panel (b) of Fig. 5 we show the highest average density of the coexistence region associated with T_u^β and $T_{max}^{Y_e=0.4}$ for the EOSs in panel (a) and find that they are clearly anti-correlated with L_{sym}.

The striking feature here is that the pasta dissolution temperature in β-equilibrium is much lower than the maximal temperature of the phase coexistence, and that the maximal temperature $T_{\rm max}^{Y_e}$ even at a modest value of $Y_e = 0.2$ is about a factor of two higher than T_u^β. For typical values of L_{sym} around 50–60 MeV, the dissolution temperature is estimated to be $T_u^\beta \simeq 4 \pm 1$ MeV. Since our analysis neglects finite size effects such as surface, Coulomb and shell effects we believe that this is an upper limit on the dissolution temperature.

It is interesting to compare our predictions with those of other works. The maximal temperature at fixed electron fraction $Y_e = 0.3(0.5)$ was estimated from a quantum molecular dynamics (QMD) simulations to be about 5(6) MeV [47]. In a similar approach and fixing $Y_e = 0.3$, the maximal temperature was found to be 6 and 9 MeV for two different nuclear EOS with $L_{sym} = 93$ and 80 MeV [49]. In addition, another temperature scale was introduced: the temperature at which the nuclear surface is blurred due to proton drip out. This characteristic temperature is qualitatively similar to the dissolution temperature T_u in our approach. It was estimated to be around 3 MeV in Ref. [47] and around 3 or 4 MeV, depending on the nuclear EOS, in Ref. [49]. These two temperature scales are lower than ours, confirming that our temperature scales shown in Fig. 5 represent upper bounds. Notice also that the value of L_{sym} of these nuclear EOS are significantly larger than the ones we considered and our results imply that the larger the value of L_{sym} the lower the temperature (see Fig. 5). This also contribute in part to explain the differences between our results and the ones of the QMC approach. Due to its computationally heavy framework, an extended model dependence of QMD in the nuclear EOS has not yet been done. A more systematic study was done based on a Thomas-Fermi approach, and the pasta phase in β-equilibrium matter was shown to melt above 5-6 MeV [50]. This again is lower than our estimate for the maximal temperature, as expected. Finally, a recent quantum calculation (Hartree-Fock) has been performed confirming that our estimate of T_u^β is an upper limit for the melting of the crust [51].

III. NEUTRINO SCATTERING

Coherent neutrino scattering from nuclei and pasta can be estimated using the two-phase Gibbs construction discussed in the preceding section if their typical size is known. The nuclear size is set by the competition between the surface and Coulomb energies, the mass number and charge of the energetically favored nuclei can be calculated by specifying the surface tension [20]. Shell effects can also play a role but we can expect their impact to be less important at the temperatures of interest, and we neglect them in the following analysis. Further, although we should expect a distribution of nuclei at finite temperature, to obtain a simple first estimate we shall assume that the distribution is dominated by a single

nucleus. In this case, the radius of the favored nucleus is [20].

$$r_A^3 = \frac{3\sigma}{4\pi e^2 (n_p^h)^2 f_3(u)} \quad \text{with} \quad f_3(u) = \frac{2 - 3u^{1/3} + u}{5}\,, \tag{4}$$

where σ is the surface tension between the low and high density phases, and $f_3(u)$ is the geometrical factor associated with the Coulomb energy of the Wigner-Seitz cell in $d = 3$ dimensions [29]. The surface tension is a function of the density, Y_e and T. We use the ansatz from Ref. [30] (see also Ref. [31]) and parameters obtained for the SLy4 interaction. Note that this simple ansatz neglects the influence of the protons in the low density gas phase on the surface tension [32] .

For the purpose of calculating coherent neutrino scattering, we shall, for simplicity, assume that nuclei are spherical for all values of u. This is reasonable because angle averaged coherent scattering rates from rod-like and slab-like structures have been calculated earlier and found to be comparable or smaller than those from spherical nuclei of similar size [33]. Further, as noted earlier, close to β-equilibrium the pasta region is relatively small even for $T < T_{\rm u}^{\beta}$, and absent for $T > T_{\rm u}^{\beta}$.

The differential coherent elastic scattering rate from the nuclei in the heterogeneous phase is given by [14, 52]

$$\frac{d\Gamma_{\rm coh}}{d\cos\theta} = \frac{G_F^2\ E_\nu^2}{8\pi}\ n_A\ (1+\cos\theta)\ S(q)\ N_{\rm w}^2\ F_A^2(q) \tag{5}$$

where the total weak charge of a nucleus is defined as [14]

$$N_{\rm w} = \frac{4\pi}{3} r_A^3\ (n_n^h - n_n^l)\,, \tag{6}$$

and $n_A = 3u/(4\pi r_A^3)$ is the density of nuclei. We have neglected the proton contribution in the vector response because of their weak charge $\simeq 1 - 4\sin^2\theta_W \approx 0$, and subtracted the density of neutrons from the low density phase because neutrinos only scatter off the density contrast. The static structure factor $S(q)$ accounts for correlations between nuclei due to long-range Coulomb interactions (weakly screened by electrons) that tends to suppress scattering at small momentum transfer $q = E_\nu\sqrt{2(1-\cos\theta)} \lesssim 1/a$ where $a = (3/4\pi n_A)^{1/3} = r_A/u^{1/3}$ is the average distance between nuclei. Scattering with high momentum transfer with $q \gtrsim 1/r_A$ is suppressed by the form factor of the nucleus $F_A(q)$ which we take to be that of a sphere of constant density and radius r_A. More realistic choices such as the Helm form factor [34], have a negligible impact on our results.

In a one component plasma, $S(q)$ depends on a and the Coulomb coupling parameter $\Gamma = Z^2e^2/ak_BT$ where Z is the ion charge, $e^2 = 1/137$ and k_BT is the thermal energy. In our simple model for the heterogeneous state where we assume a single spherical nucleus captures the essential physics and ^{56}Fe being the ground state at zero density,

$$Z \approx 26\ \left(\frac{\sigma}{\sigma_0}\right)\ \left(\frac{n_0}{2n_p^h}\right)\ \left(\frac{f_3(0)}{f_3(u)}\right)\,, \tag{7}$$

where we used Eq. (4) and the following parameters: $\sigma_0 \simeq 1.2$ MeV/fm^2 is the surface tension of symmetric nuclei in vacuum, $n_0 \simeq 0.16$ fm^{-3} is the nuclear saturation density. Typically we find $Z \simeq 50$ at the density for which we expect an appreciable fraction of large nuclei or pasta, and $\Gamma \gg 1$. For large Γ the static structure factor $S(q) \ll 1$ unless $qa \gg 1$, and for $\Gamma > 10$ the interference of amplitudes for neutrino scattering off different clusters is strong and destructive at small $qa < 2$–3. At intermediate $qa \simeq 4$–5, constructive interference can enhance scattering, and for $qa \gg 5$ where interference is negligible $S(q) \simeq 1$. In this work we employ $S(q)$ obtained from recent fits to accurate MD simulations of one-component plasmas [35] to properly account for screening for Γ in the range 1–150. We note that for $T > 2$ MeV, $\Gamma < 150$ even at the highest density, and crystallization is not favored and its reasonable to work with $S(q)$ obtained for the liquid state.

The neutrino scattering rate from non-relativistic nucleons in the gas phase is given by [53]

$$\frac{d\Gamma_\nu}{d\cos\theta} = \frac{G_F^2\ E_\nu^2}{8\pi}\ \sum_{ij}\Big[(1+\cos\theta)\ C_v^i C_v^j S_v^{ij}(q) + (3-\cos\theta) C_a^i C_a^j S_a^{ij}(q)\Big]\,, \tag{8}$$

where the labels i and j can be either neutrons or protons, C_v^i and C_a^i are their corresponding vector and axial vector charges. In the long-wavelength limit, which is adequate to describe low energy neutrino scattering, the static structure factors (unnormalized) can be related to thermodynamic functions [46],

$$S_v^{ij} = T\left(\frac{\partial^2 P}{\partial\mu_j\partial\mu_i}\right)_T \tag{9}$$

where P is the pressure of the gas phase and μ_i is the chemical potential of either neutrons or protons, and the axial or spin response

$$S_a^{ij} = T\left(\frac{\partial^2 P}{\partial\delta_j\partial\delta_i}\right)_T\,, \tag{10}$$

where δ_i is the chemical potential associated with the spin density of species i. When interactions between nucleons can be neglected, the structure functions greatly simplify and are given by

$$S_v^{ij} = S_a^{ij} = \delta^{ij} S_{gas}(\mu_i, T)\,, \tag{11}$$

where [54]

$$S_{gas}(\mu_i, T) = \int \frac{d^3p}{(2\pi)^3}\ \frac{e^{\beta(p^2/2m-\mu_i)}}{(1+e^{\beta(p^2/2m-\mu_i)})^2}\,, \tag{12}$$

where $\beta = 1/T$ and only correlations due to Fermi statistics are included. Strong nuclear interactions induce additional correlations between nucleons in the gas and can alter the structure factors. At the sub-nuclear densities

of interest, calculations suggest a modest enhancement of the vector response, and a suppression by up to 50% of the axial response [36–40]. Since our primary interest here is to asses the role of coherent scattering, in what follows we shall neglect corrections due to strong interactions and use Eq. (11) to calculate the scattering rates in the gas phase.

To asses the importance of coherent scattering from heavy nuclei in the heterogeneous phase we define the ratio

$$\mathcal{R} = \frac{\sigma^{\rm tran}_{het}(E_\nu)}{\sigma^{\rm tran}_{hom}(E_\nu)} = \frac{\sigma^{\rm tran}_{coh}(E_\nu) + \sigma^{\rm tran}_{gas}(E_\nu)}{\sigma^{\rm tran}_{hom}(E_\nu)} = \frac{n_A N_{\rm w}^2 \langle S_{cl}(E_\nu)\rangle + (1+5(C_A^n)^2) S_{gas}(\mu_n^{het},T) + 5(C_A^p)^2 S_{gas}(\mu_p^{het},T)}{(1+5(C_A^n)^2) S_{gas}(\mu_n^{hom},T) + 5(C_A^p)^2 S_{gas}(\mu_p^{hom},T)}\,, \tag{13}$$

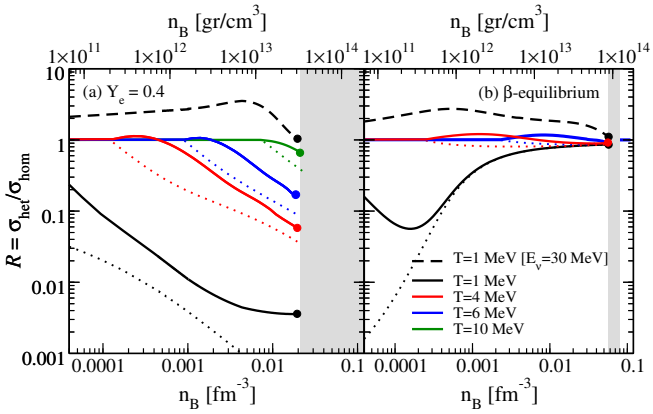

FIG. 6. Ratio $\mathcal{R}$ from Eq.(13) in two different conditions: (a) fixed proton fraction $Y_e = 0.4$ and (b) β-equilibrium (right panel). The gray band indicates the region in density where non-spherical pasta may be present, and the curves terminate with a dot for the density at which $u = 1/8$. Dotted curves indicate the contribution of the external gas only. Neutrino are considered at thermal equilibrium, except for the black dashed curves where $E_\nu = 30$ MeV.

where $\sigma^{\rm tran} = \int d\cos\theta\ (1-\cos\theta)\ d\Gamma/d\cos\theta$ is the elastic transport cross section per unit volume for neutrinos. $\mathcal{R}$ is analogous to the parameter ξ introduced in [17], and quantifies the change in neutrino scattering rates in heterogeneous phase, where both coherent scattering from nuclei ($\sigma^{\rm tran}_{coh}$) and scattering from free nucleons in the gas phase contribute. The term $\langle S_{cl}(E_\nu)\rangle$ in the cross section from clusters indicates angle averaging of the corrections due to correlations and nuclear form factors [17],

$$\langle S_{cl}(E_\nu)\rangle = \frac{3}{4}\int_{-1}^{1} d\ \cos\theta(1-\cos\theta)(1+\cos\theta) S(q)\ F_A^2(q) \tag{14}$$

and is a function of E_ν trough $q = E_\nu\sqrt{2(1-\cos\theta)}$. We note that neglecting both the correlations in the gas and the protons has a small impact of $\lesssim 10\%$ on the ratio. However, a strong suppression of the nucleon axial response due to spin correlations would reduce the opacity of the homogeneous phase, and favor larger $\mathcal{R}$.

The results for the ratio of cross section $\mathcal{R}$ are displayed in Fig. 6. Panel (a) show results at fixed proton fraction $Y_e = 0.4$ and on panel (b) results for matter in β-equilibrium are shown. In both cases, with the exception of the black dashed line, neutrinos are assumed to be thermal and their energy $E_\nu = 3T$. The energy dependence of the cross sections is shown in Fig. 7. The strong suppression of coherent scattering at low energy is clearly visible, and the dot on each curve corresponding to $E_\nu = 3T$ shows that Coulomb correlation suppresses scattering for neutrino energies of interest. The Coulomb parameter Γ for the plots in Fig. 7 range from $\Gamma_{\rm min} = 4(6)$ for $n_B = 0.01$ fm^{-3} and $T = 10(6)$ MeV to $\Gamma_{\rm max} = 150(74)$ for $u = 1/8$ and $T = 1$ MeV at fixed proton fraction (beta-equilibrium). The value of Γ at select points is shown in Table I. At the lowest temperature of $T = 1$ MeV and large proton fraction $Y_e = 0.4$, our simple ansatz in Eq. 7 predicts a large $Z > 60$ and $\Gamma > 200$. At these very low temperatures, it would be appropriate to use $S(q)$ from simulations of the solid phase. However, here we adopt the approximate treatment suggested in earlier studies [19, 41] where they circumvent the problem by limiting the value of the Coulomb coupling to $\Gamma_{max} = 150$, and is indicated by an asterisk in Table I. These low temperature conditions are encountered only at late times in the proto-neutron star phase when the neutrino luminosity is greatly reduced and undetectable even for close by supernovae in detectors such SuperKamiokande where energy threshold is about 5 MeV. Additionally, shell effects can be important in the determination of Z at low temperature and smaller values of $Z \approx 40-50$ are obtained at $T = 0$ [21, 42]. Nonetheless, we included these low temperature results, which despite the approximations mentioned, provide useful insights about trends and allow for comparison with earlier work.

A related quantity of interest to neutrino transport are the diffusion coefficients

$$D_n = \int_0^\infty dx x^n \lambda(E_\nu) f(E_\nu)\,[1-f(E_\nu)] \tag{15}$$

with $x = E_\nu/T$ and f the Fermi-Dirac distribution [4]. Results for D_2 and D_4 at $T = 4$ MeV and $n_B = 0.01$ fm^{-3} for both β-equilibrium and fixed $Y_e = 0.4$ are presented in Table II assuming that the neutrino chemical potential μ_ν is negligible. In the first row we also show the result for

TABLE I. Values of neutrino mean-free-path and diffusion coefficients at $T = 4$ MeV and $n_B = 0.01$ fm^{-3}.

	HOM $Y_e = 0.4$	HET $Y_e = 0.4$	HOM β	HET β
$\lambda(E_\nu = 3T)$ [m]	14.91	98.03	14.19	14.87
D_2 [m]	67.01	575.01	63.77	74.47
D_4 [m]	220.79	1326.91	210.12	208.71

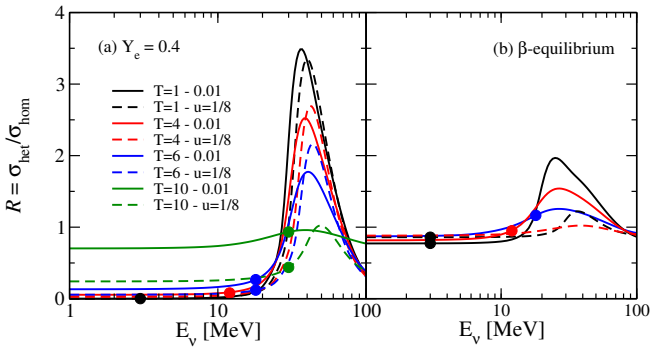

FIG. 7. Energy dependence of the total ratio of cross section $\mathcal{R}$ at various temperatures and for two different densities: $n_B = 0.01$ fm^{-3} (full lines) and the threshold density for which $u = 1/8$ (dashed lines). As for Fig.6 panel (a) is for fixed proton fraction $Y_e = 0.4$ and panel (b) for β-equilibrium conditions. In both cases the full dots indicate the energy for thermal neutrinos ($E_\nu = 3T$).

the mean-free-path $\lambda(E_\nu) = 1/\sigma(E_\nu)$ at $E_\nu = 3T$. These results are compatible with the general trend observed in the results above that predict little effects of pasta at beta equilibrium and a reduced scattering at fixed proton fraction.

From Figs. 6 and 7 we can draw the following conclusions:

- At low temperature when large nuclei are present and persist up to high density, the opacity to high energy neutrinos with $E_\nu \gtrsim 4/a$ where a the distance between nuclei is enhanced, but coherent scattering is greatly reduced for low energy thermal neutrinos due to Coulomb correlations between nuclei. We find a net reduction in the scattering rates in the heterogeneous phase because a large fraction of free nucleons are tied up inside nuclei. In the homogeneous phase these nucleons make a significant contribution to neutrino scattering because they couple to the axial current.

TABLE II. Values of Coulomb coupling Γ for Fig. 7.

T in MeV	$n_B = 0.01$ $Y_e = 0.4$	$u = 1/8$ $Y_e = 0.4$	$n_B = 0.01$ β	$u = 1/8$ β
1	150*	150*	72.7	74.0
4	69.8	138.8	14.2	4.0
6	35.1	75.4	6.3	–
10	4.0	17.4	–	–

- In β-equilibrium coherent scattering makes a relatively small contribution to the total neutrino opacity for all temperatures of interest. At low temperature, when nuclei and pasta are present, Coulomb correlations reduce coherent scattering, and at high temperature, pasta and large nuclei melt. We find that scattering off nucleons in the gas phase dominates unless nuclear correlations can greatly suppress the spin response of dilute nuclear matter.

- Large opacity due to coherent scattering reported in Ref. [17] arose because the neutrino energy was chosen to be large to ensure that the suppression due to Coulomb correlations was mild, and it was assumed that pasta nuclei would survive up to $T \simeq 10$ MeV in matter close to β-equilibrium.

- Fig. 7 illustrates that the heterogeneous phases can act as a low-pass filter for neutrinos. In the diffusive regime the strong energy dependence of the neutrino cross-sections would imply non-linear thermal evolution where cooling would accelerate rapidly with decreasing temperature.

These results have significant implications for the impact of coherent pasta scattering on proto-neutron star cooling. In Ref. [17], it was shown that if coherent scattering from nuclear pasta increases the neutrino opacity relative to that of a homogeneous gas, pasta formation in the outer layers of the proto-neutron star can trap neutrino energy for the first few seconds after a successful core collapse supernova explosion. This heat trapping causes the temperature of the outer layers of the proto-neutron to increase until they reach the pasta melting temperature. This heats up the entire region over which neutrinos decouple from matter, increasing the average energy of neutrinos escaping from the proto-neutron star. Additionally, the energy that is trapped initially gets out at later times. Both of these effects contributed to a more detectable late-time neutrino signal. A pasta melting temperature of 10 MeV was used in their parameterized simulations, but it was suggested that reducing the melting temperature of the pasta could reduce the impact of the pasta on the neutrino signal.

Here, we have found that the pasta dissolution temperature for β-equilibrated matter is $T_{\rm u}^{\beta} \approx 4 \pm 1$ MeV and that the presence of a high-density phase can reduce the neutrino opacity. First, this implies that even if coherent scattering from nuclear pasta increased the neutrino opacity, the impact of pasta on the proto-neutron star neutrino signal would be smaller than the impact predicted by Ref. [17], since nuclear pasta would be present for a shorter portion of proto-neutron star cooling. The reduced melting temperature would also cause a smaller perturbation in the temperature gradient near the neutrino sphere, which would reduce the enhancement of the neutrino luminosity even when the pasta is present. Second, we predict that correlations among high-density structures act to reduce the neutrino opacity for neutrinos with energies $\lesssim 4/a$, which is an energy scale that is

often significantly above the thermal energy. Therefore, the presence of pasta may allow the majority of thermal neutrinos to escape more easily and potentially speed up neutrino cooling, thereby reducing the late-time neutrino detection rate from a nearby supernova.

IV. CONCLUSIONS

In this paper, we have analyzed the properties of the hot nuclear pasta phase and we have shown the large qualitative differences between matter in β-equilibrium and at modest electron fraction $Y_e > 0.2$. In beta-equilibrium, we find that pasta melts or dissolves at relatively low temperature, reducing drastically the volume fraction occupied by the large nuclei. With increasing temperature protons leak out of nuclei, enter the gas phase and alter the nature of the transition to bulk matter. Here, nuclei dissolve with increasing density in a phenomena referred to as retrograde condensation. We have introduced a new temperature, the pasta dissolution temperature $T_{\rm u}$, above which the volume fraction of nuclei cannot exceed 1/8. In β-equilibrium the dissolution temperature $T_{\rm u}^{\beta} \simeq 4 \pm 1$ MeV for EOS with $L_{sym} = 50 - 60$ MeV and compatible with EFT predictions in neutron matter. The dissolution temperature $T_{\rm u}^{\beta}$ was found to decrease with increasing L_{sym}. For matter with $Y_e > 0.2$ large nuclei and pasta persist to higher temperatures $T_{\rm u} \simeq 15$ MeV and retrograde condensation is absent. Our work confirms results obtained in earlier work in Refs. [47, 49] and expands on them by delineating the mechanism and defining a dissolution temperature $T_{\rm u}$ to provide an upper limit for any equation of state independent of finite size corrections.

In the second part of our paper, we have analyzed the impact of the coherent scattering off nuclear clusters on the neutrino opacities, for thermodynamical conditions corresponding to core-collapse supernovae or neutron star mergers. We found that both the retrograde condensation and the Coulomb correlations in the static structure factor contribute to reduce the impact of coherent scattering on neutrino opacities. For matter far out of beta-equilibrium where heavy nuclei and pasta persist to high temperatures, Coulomb correlations between clusters greatly reduce the coherent scattering rates at high density. Here, rather than an increase, we found a net reduction in the opacity for thermal neutrinos when clusters are present. This may be important at very early times post bounce during the supernova when matter with large Y_e is encountered briefly during the period when lepton number is trapped. On longer timescales characteristic of proto-neutron star evolution, beta-equilibrium favors much smaller values of Y_e, and for $T < T_{\rm u}^{\beta}$ only a moderate increase by less than 20% is found for thermal neutrinos, at variance with the factor 5 reported in Ref. [17]. We find such an increase only for high energy non-thermal neutrinos, for which correlations between nuclei enhance the scattering rates.

While we believe the physical effects mentioned above are robust, additional work is warranted to obtain more quantitative predictions. Hartree-Fock calculations, such as those being reported in Ref. [43, 44] which self-consistently include the surface tension, Coulomb, and shell effects, would provide improved estimates for $T_{\rm u}^{\beta}$ to better constrain the temperature range in which pasta is present. It will also be desirable to go beyond the single-nucleus approximation in calculating the ion structure factor, and include in addition non-spherical shapes. Ultimately, these modifications to the neutrino opacities need to be incorporated self-consistently with the underlying equation of state in proto-neutron star and supernova simulations to asses if the presence of nuclear clusters at sub-nuclear density can influence supernova observables. Nonetheless, it seems likely that retrograde condensation and ion-correlations will together disfavor the large changes to the temporal structure of the neutrino signal predicted in Ref. [17].

V. ACKNOWLEDGEMENTS

We would like to thank C. Horowitz and W. Newton for discussions. SR was supported by DOE Grant No. DE-FG02-00ER41132. AR was supported by NSF Grant No. AST-1333607 and by DOE Grant No. DE-AC52-06NA25396. LR was supported by the DOE Office of Science under Award No. DE-SC0017955. JM was partially supported by the IN2P3 Master Project MAC.

[1] A. Burrows, Reviews of Modern Physics **85**, 245 (2013).
[2] H.-T. Janka, Annual Review of Nuclear and Particle Science **62**, 407 (2012).
[3] A. Burrows and J. M. Lattimer, Astrophys.J. **307**, 178 (1986).
[4] J. A. Pons, S. Reddy, M. Prakash, J. M. Lattimer, and J. A. Miralles, The Astrophysical Journal **513**, 780 (1999).
[5] T. Fischer, I. Sagert, G. Pagliara, M. Hempel, J. Schaffner-Bielich, T. Rauscher, F.-K. Thielemann, R. Käppeli, G. Martínez-Pinedo, and M. Liebendörfer, The Astrophysical Journal Supplement Series **194**, 39 (2011).
[6] L. F. Roberts and S. Reddy, "Neutrino signatures from young neutron stars," in Handbook of Supernovae, edited by A. W. Alsabti and P. Murdin (Springer International Publishing, Cham, 2016) pp. 1–31.
[7] L. Hüdepohl, B. Muller, H.T. Janka, A. Marek, G.G. Raffelt, Phys. Rev. Lett. **104**, 251101 (2010).
[8] T. Fischer, G. Martínez-Pinedo, M. Hempel, and M. Liebendörfer, Phys. Rev. D **85**, 083003 (2012)..

[9] L. F. Roberts, G. Shen, V. Cirigliano, J. A. Pons, S. Reddy, and S. E. Woosley, Phys. Rev. Lett. **108**, 061103 (2012).
[10] G. Martínez-Pinedo, T. Fischer, A. Lohs, and L. Huther, Phys. Rev. Lett. **109**, 251104 (2012).
[11] S. Wanajo, Astro. J. Lett. **770**, L22 (2013).
[12] D. Z. Freedman, Phys. Rev. **D9**, 1389 (1974).
[13] N. K. Glendenning, Phys. Rev. **D46**, 1274 (1992).
[14] S. Reddy, G. Bertsch, and M. Prakash, Phys. Lett. **B475**, 1 (2000).
[15] C. J. Horowitz, M. A. Perez-Garcia, and J. Piekarewicz, Phys. Rev. **C69**, 045804 (2004).
[16] H. Sonoda, G. Watanabe, K. Sato, T. Takiwaki, K. Yasuoka, and T. Ebisuzaki, Phys. Rev. C **75**, 042801 (2007).
[17] C. J. Horowitz, D. K. Berry, M. E. Caplan, T. Fischer, Z. Lin, W. G. Newton, E. O'Connor, and L. F. Roberts, arXiv:1611.10226 [astro-ph.HE].
[18] N. Itoh, Progress of Theoretical Physics **54**, 1580 (1975).
[19] N. Itoh, R. Asahara, N. Tomizawa, S. Wanajo, and S. Nozawa, The Astrophysical Journal **611**, 1041 (2004).
[20] C. J. Pethick and D. G. Ravenhall, Ann. Rev. Nucl. Part. Sci. **45**, 429 (1995).
[21] F. Douchin and P. Haensel, Astronomy and Astrophysics **380**, 151 (2001).
[22] J. M. Pearson, N. Chamel, S. Goriely, and C. Ducoin, Physical Review C **85**, 065803 (2012).
[23] W. G. Newton and J. R. Stone, Phys. Rev. C **79**, 055801 (2009).
[24] S. S. Avancini, D. P. Menezes, M. D. Alloy, J. R. Marinelli, M. M. W. Moraes, and C. Providência, Phys. Rev. C **78**, 015802 (2008).
[25] C. Ducoin, P. Chomaz, and F. Gulminelli, Nuclear Physics A **771**, 68 (2006).
[26] H. Muller and B. D. Serot, Phys. Rev. **C52**, 2072 (1995).
[27] I. Tews, S. Gandolfi, A. Gezerlis, and A. Schwenk, Phys. Rev. C **93**, 024305 (2016).
[28] C. Drischler, K. Hebeler, and A. Schwenk, Phys. Rev. C **93**, 054314 (2016).
[29] D. G. Ravenhall, C. J. Pethick, and J. R. Wilson, Phys. Rev. Lett. **50**, 2066 (1983).
[30] A. da Silva Schneider, L. F. Roberts, and C. D. Ott, arXiv:1707.01527 [astro-ph.HE].
[31] J. Lattimer, C. Pethick, D. Ravenhall, and D. Lamb, Nuclear Physics A **432**, 646 (1985).
[32] F. Aymard, F. Gulminelli, and J. Margueron, Physical Review C **89**, 065807 (2014).
[33] P. Alcain and C. Dorso, Nuclear Physics A **961**, 183 (2017).
[34] R. H. Helm, Phys. Rev. **104**, 1466 (1956).
[35] N. Desbiens, P. Arnault, and J. Clérouin, Physics of Plasmas **23**, 092120 (2016).
[36] N. Iwamoto and C. J. Pethick, Phys. Rev. **D25**, 313 (1982).
[37] A. Burrows and R. F. Sawyer, Phys. Rev. **C58**, 554 (1998).
[38] S. Reddy, M. Prakash, J. M. Lattimer, and J. A. Pons, Phys. Rev. **C59**, 2888 (1999).
[39] C. J. Horowitz and A. Schwenk, Phys. Lett. **B642**, 326 (2006).
[40] C. J. Horowitz, O. L. Caballero, Z. Lin, E. O'Connor, and A. Schwenk, Phys. Rev. **C95**, 025801 (2017)NoStop
[41] C. J. Horowitz, Phys. Rev. D **55**, 4577 (1997).
[42] M. Onsi, A. K. Dutta, H. Chatri, S. Goriely, N. Chamel, and J. M. Pearson, Phys. Rev. C **77**, 065805 (2008).
[43] W. G. Newton and J. R. Stone, Phys. Rev. **C79**, 055801 (2009).
[44] B. Schuetrumpf, C. Zhang, and W. Nazarewicz, in Nuclear Particle Correlations and Cluster Physics, edited by W.-U. Schröder (2017) pp. 135–153
[45] N. Glendenning, Compact Stars, second edition (Springer 1997) .
[46] K. Huang, Statistical Mechanics, Second Edition, John Wiley & Sons (1987).
[47] G. Watanabe, K. Sato, K. Yasuoka, and T. Ebisuzaki, Phys. Rev. C 69, 055805 (2004); Erratum Phys. Rev. C 81, 049901(E) (2010).
[48] S. S. Avancini, S. Chiacchiera, D. P. Menezes, and C. Providência, Phys. Rev. C 82, 055807 (2010); Erratum Phys. Rev. C 85, 059904(E) (2012).
[49] Hidetaka Sonoda, Gentaro Watanabe, Katsuhiko Sato, Kenji Yasuoka, and Toshikazu Ebisuzaki, Phys. Rev. C 77, 035806 (2008); Erratum Phys. Rev. C 81, 049902(E) (2010).
[50] F. Grill, H. Pais, C. Providência, I. Vidaña, and S. S. Avancini, Phys. Rev. C 90, 045803 (2014).
[51] W. Newton, in preparation.
[52] R.F. Sawyer, Phys. Rev. D 11, 2740 (1975).
[53] N. Iwamoto & C.J. Pethick, Phys. Rev. D 25, 313 (1982).
[54] A.L. Fetter & J.D. Walecka, Quantum Theory of Many-Particle Systems, Dover Publications (New-York, 1971).